Effect of complex climatic and wheel load conditions on resilient modulus of unsaturated subgrade soil

Daoju Ren [i], Tatsuya Ishikawa [ii)*], Junling Si [iii], Tetsuya Tokoro [iv]

[i] **Daoju Ren, Doctoral Student**
Graduate School of Engineering, Hokkaido University, Kita 13, Nishi 8, Kita-ku, Sapporo 060-8628, Japan
e-mail: daoju.ren.d5@elms.hokudai.ac.jp

[ii] **Tatsuya Ishikawa, Professor** (*Corresponding author*)
Faculty of Engineering, Hokkaido University, Kita 13, Nishi 8, Kita-ku, Sapporo 060-8628, Japan
e-mail: t-ishika@eng.hokudai.ac.jp

[iii] **Junling Si, Doctoral Student**
Graduate School of Engineering, Hokkaido University, Kita 13, Nishi 8, Kita-ku, Sapporo 060-8628, Japan
e-mail: junling.si.h3@elms.hokudai.ac.jp

[iv] **Tetsuya Tokoro, Associate Professor**
Faculty of Engineering, Hokkai-Gakuen University, 1-1, Minami 26, Nishi 11, Chuo-ku, Sapporo 064-0926, Japan
e-mail: tokoro@cvl.hokkai-s-u.ac.jp

Abstract

Resilient modulus (M_r) is a fundamental mechanical property vital for assessing the resistance of pavement structures to cyclic vertical loads. It has played a pivotal role in pavement design and has been instrumental in predicting pavement responses and fatigue life. The M_r of subgrade soil is affected by a multitude of factors, including stress, moisture, and temperature conditions, all of which interact to define the response of the soil. This research investigated the effect of complex climatic conditions on M_r with a particular focus on areas experiencing significant seasonal changes in snowy cold regions like Hokkaido, Japan. Previous studies have proposed predictive models for M_r, incorporating the concept of matric suction, to account for moisture conditions. However, these models have rarely considered suction hysteresis in the soil-water characteristic curve (SWCC) or the effects of wheel loading on frost-susceptible subgrade soil during different seasons. In this study, a series of M_r tests were conducted on two types of subgrade soil under various climatic and wheel loading conditions. The test results promise to enhance our understanding of the complex interplay of climatic and stress conditions on M_r of standard sand and frost susceptible subgrade soil along different drying and wetting paths, particularly in regions with significant seasonal variations.

Keywords: Resilient modulus; Unsaturated subgrade soil; Suction hysteresis; Freeze-thaw; Wheel load; Predictive model.

1 Introduction

Resilient modulus, M_r, originally defined as the ratio of the cyclic deviator stress to the resilient axial strain during cyclic loading by Seed et al. (1955), is a crucial mechanical characteristic used to assess the resistance of pavement structures to cyclic vertical loads. It has been widely used in pavement design works since the publication of the *AASHTO Guide for Design of Pavement Structures* (AASHTO, 1986), and plays a major role in determining pavement responses and fatigue life (Li & Selig, 1994; Brown, 1996; Kim & Kim, 2007). Furthermore, the M_r of subgrade soil is affected by many factors, including stress, moisture, and temperature conditions, which comprehensively interact to define the response of the soil (Johnson et al., 1978; Cole et al., 1981; Berg et al., 1996; Simonsen and Isacsson, 2001; Simonsen et al., 2002).

The current Mechanistic-Empirical Pavement Design Guide (MEPDG) utilizes a universal model for predicting M_r under different stress conditions and considers the effect of moisture fluctuation by estimating the ratio of M_r to M_r at optimum moisture content (NCHRP, 2004; AASHTO, 2020). Many researchers also proposed M_r predictive models by incorporating the concept of matric suction based on the universal model of MEPDG to capture the effect of moisture conditions (Lytton, 1996; Heath et al., 2004; Gupta et al., 2007; Liang et al., 2008; Khoury et al., 2009; Oh et al., 2012; Ng et al., 2013; Sahin et al., 2013; Gu et al., 2015). In addition, MEPDG also estimates the climatic effects on pavement materials, responses, and distress of climate using the Enhanced Integrated Climatic Model (EICM) in an integrated manner (AASHTO, 2020). However, as this model only estimates the climatic effects by adjusting the overall magnitude of the universal M_r predictive model, it lacks theoretical explanations for the effects of freeze-thaw action. Therefore, the comprehensive effect of the complex climatic conditions on the M_r of subgrade soils needs to be further studied.

In areas with significant seasonal changes in snowy cold regions such as Hokkaido, a northern island in Japan, the effect of complex climatic conditions on M_r cannot be ignored (Ishikawa et al., 2019; Lin et al., 2022). To investigate the effect of climatic conditions including moisture and temperature changes, Lin et al. (2022) conducted M_r tests under different combinations of the conditions and proposed a modified M_r predictive model able to capture the effects of moisture and freeze-thaw action comprehensively based on the Ng model (Ng et al., 2013). However, the effect of the suction hysteresis of SWCC and the difference between the drying and wetting paths were not considered, and the effects of wheel loading during different seasons also need to be further understood. In this study, a series of M_r tests for two types of subgrade soil with different frost susceptibility under different climatic and wheel loading conditions were conducted to investigate the effect of complex climatic and stress conditions on the M_r of subgrade soils, especially under the effect of suction hysteresis.

2 M_r predictive model

MEPDG (AASHTO, 2020) recommends the test protocol of the AASHTO T 307 (AASHTO, 2017) to measure the M_r and fit the results by the generalized predictive model shown as follows:

$$M_r = k_1 p_a \left(\frac{\theta}{p_a}\right)^{k_2} \left(\frac{\tau_{oct}}{p_a} + 1\right)^{k_3} \tag{1-1}$$

$$\theta = \sigma_1 + \sigma_2 + \sigma_3 \tag{1-2}$$

$$\tau_{oct} = \frac{1}{3}\sqrt{(\sigma_1 - \sigma_2)^2 + (\sigma_1 - \sigma_3)^2 + (\sigma_2 - \sigma_3)^2} \tag{1-3}$$

where k_1, k_2, and k_3 are regression parameters; σ_1, σ_2, and σ_3 are major principal stress, intermediate principal stress, and minor principal stress, respectively; p_a is atmospheric pressure and set as 101 kPa in this study; θ is bulk stress; τ_{oct} is octahedral stress.

Guide for Mechanistic-Empirical Design of New and Rehabilitated Pavement Structures reported the estimation method for the effect of changing moisture content as shown in the following equation (NCHRP, 2004):

$$\log\frac{M_r}{M_{ropt}} = a + \frac{b-a}{1+EXP\left[\ln\left(-\frac{b}{a}\right)+k_m(S-S_{opt})\right]} \tag{2}$$

where S is the degree of saturation in decimals; S_{opt} is the degree of saturation at optimum moisture content in decimals; a is the minimum of $log\ (M_r/M_{ropt})$; b is the maximum of $log\ (M_r/M_{ropt})$; k_m is regression parameter.

However, **Eq. 2** lacks the mechanical explanation of unsaturated soil, and its applicability to other regions may not be good because the empirical equation is based on the field data in the USA. Han & Vanapalli (2016) summarized a series of predictive models for unsaturated subgrade soils and indicated that the Ng model (Ng et al., 2013) shown in **Eq. 3** has a relatively high accuracy:

$$M_r = k_1 p_a \left(\frac{\theta}{p_a}\right)^{k_2} \left(\frac{\tau_{oct}}{p_a} + 1\right)^{k_3} \left(\frac{\psi}{\sigma_{net}} + 1\right)^{k_4} \tag{3}$$

where k_4 is regression parameter; σ_{net} is net mean stress, defined as (θ/3-u_a); ψ is matric suction. It should be noted that the octahedral shear stress τ_{oct} is used in **Eq. 3** instead of the cyclic deviator stress q_{cyc} in the original form of the Ng model. According to the definition of octahedral shear stress, when $\sigma_2 = \sigma_3$, $\tau_{oct} = \frac{\sqrt{2}}{3}(\sigma_1 - \sigma_3)$. Considering the regression parameters, using the octahedral shear stress or the deviator stress does not affect the fitting result. Furthermore, since MEPDG uses octahedral shear stress in its predictive model, the Ng model is converted to the current form to keep the consistency.

Based on **Eq. 3**, Lin et al. (2022) proposed a modified model to capture both the effects of moisture content and freeze-thaw action by incorporating a new parameter F_{clim} multiplying k_1 to k_4:

$$M_r = F_{clim} \cdot k_1 p_a \left(\frac{\theta}{p_a}\right)^{F_{clim} \cdot k_2} \left(\frac{\tau_{oct}}{p_a} + 1\right)^{F_{clim} \cdot k_3} \left(\frac{\psi}{\sigma_{net}} + 1\right)^{F_{clim} \cdot k_4} \quad (4)$$

where F_{clim} is the climatic factor. This model not only captures the effect of freeze-thaw action on the overall magnitude of the M_r surface in the σ_d-σ_c-M_r 3D space but also reflects the change of the surface shape, which will be employed to investigate the effect of complex climatic and stress conditions on M_r in the later sections of this paper.

3 Test materials

Two types of soil are used in this study: Toyoura sand (Japanese standard sand) and subgrade soil sampled from the site. The subgrade soil is sampled from an experimental road located at Tomakomai, Hokkaido, Japan (hereinafter referred to as Tomakomai soil), which is a kind of volcanic soil with a relatively small density. According to the Unified Soil Classification System of ASTM (2017), Toyoura sand is classified as SP, poorly graded sand; and Tomakomai soil is classified as SM, silty sand. The physical properties and the grain size distribution curves are shown in **Table 1** and **Fig. 1**, respectively. It should be noted that according to the standard of AASHTO T 307-99 (AASHTO, 2017), the particles exceeding 25% of the available largest mold diameter should be removed in this study to fit the test apparatus size. The specimens are compacted to reach a degree of compaction of 95%, corresponding to a dry density of 1.54 g/cm^3 for Toyoura sand and 1.21 g/cm^3 for Tomakomai soil to satisfy the quality control of the subgrade layer in asphalt pavement provided by Japan Road Association (2019). Tomakomai soil is a type of frost susceptible soil, also named SFG subgrade material. According to the frost susceptibility test of JGS 0172 (Japanese Geotechnical Society, 2018), the frost susceptibility of Tomakomai soil is at a medium level (Yasuoka et al., 2021). On the other hand, Toyoura sand is non-frost susceptible.

Table 1 Physical properties of Toyoura sand and Tomakomai soil

Material	Soil particle density (g/cm^3)	Maximum dry density (g/cm^3)	Optimum water content (%)	Mean particle size (mm)	Fine fraction content (%)
Toyoura sand	2.65	1.62	14.0	0.19	0.7
Tomakomai soil	2.64	1.27	32.0	0.68	21.0

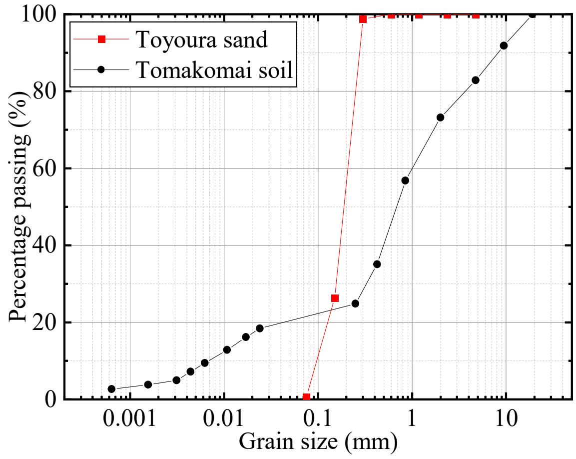

Fig. 1. Grain size distribution curves

The water retention test based on the concept of the pressure plate method is conducted in this study to obtain the soil-water characteristic curve (SWCC) of the test materials. Generally, the testing time is very long to obtain both the drying path and wetting path of the SWCC. To improve the experimental efficiency, a continuous pressurization water retention test method developed by Hatakeyama et al. (2015) as shown in **Fig. 2** is used in this study. This apparatus is based on the axis-translation method (Hilf, 1956) and has been confirmed by studies to have the same accuracy as the traditional stage pressurization method (Kato et al., 2015; Alowaisy et al., 2020; Kim et al., 2020).

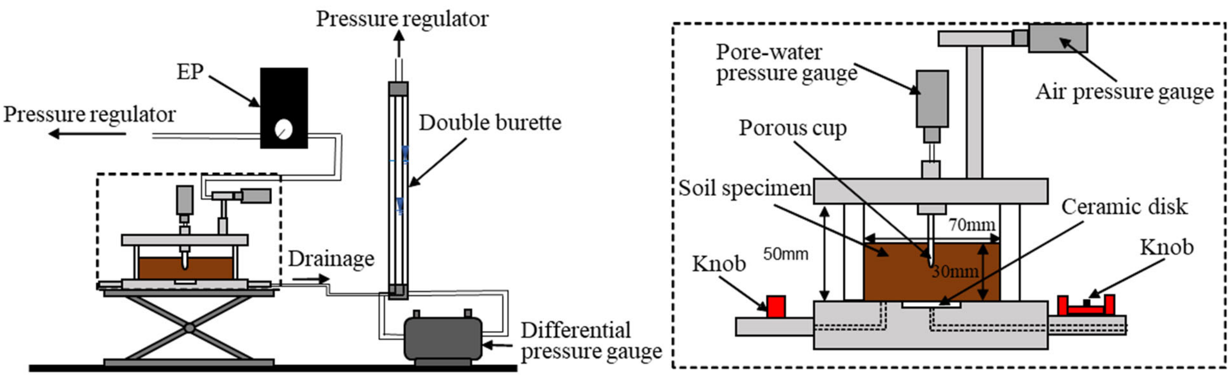

Fig. 2. Water retention test apparatus by continuous pressurization method

Fig. 3 shows the SWCCs of Toyoura sand and Tomakomai soil, fitted by the VG model (VanGenuchten, 1980). It can be found that the drying and wetting paths of SWCCs are different, namely "suction hysteresis", which is due to the 'ink bottle effect' induced by the differences in pore sizes of soils (Lu & Likos, 2004; Fredlund et al., 2012). Besides, for one certain suction value, the degree of saturation S_r differs along different scanning curves. However, the field SWCC may have experienced complicated drying and wetting cycles in history. To find the path closest to the current field condition, several scanning curves shown in **Fig. 3** (b) are measured in this study to compare with the moisture condition of the field tests. According to the long-term field measurement data (Ishikawa et al., 2019), the average S_r of the subgrade soil is 38%. Furthermore, by calculating the corresponding suction of the base course (C-40), the estimated groundwater level at the site is approximately 2 m (Lin et al., 2021). Considering the thickness of the pavement surface and base course layers, the suction at the subgrade soil surface is approximately 12 kPa. For Tomakomai soil, it can be found that the wetting scanning curve with the maximum suction ψ_{max} of 70 kPa agrees well with the field condition as shown in **Fig. 3** (b). As a result, this curve is employed in this study to represent the wetting SWCC of the Tomakomai soil. For Toyoura sand, the main drying and main wetting paths are used because the SWCC reaches the residual state when ψ_{max} = 8 kPa based on the fitting by the VG model (VanGenuchten, 1980). In this case, ψ = 3.75 kPa corresponding to S_r = 38% along the drying path is selected as the field condition for Toyoura sand to keep the consistency of the previous study (Lin et al., 2022). Furthermore, corresponding S_r and ψ along drying and wetting paths as shown in **Table 2** are selected to investigate the effect of suction hysteresis on M_r in the later chapter. It is noted that the difference of the S_r between the triaxial test and SWCC may be ± 2% ~ 4% due to the random error and the different apparatus.

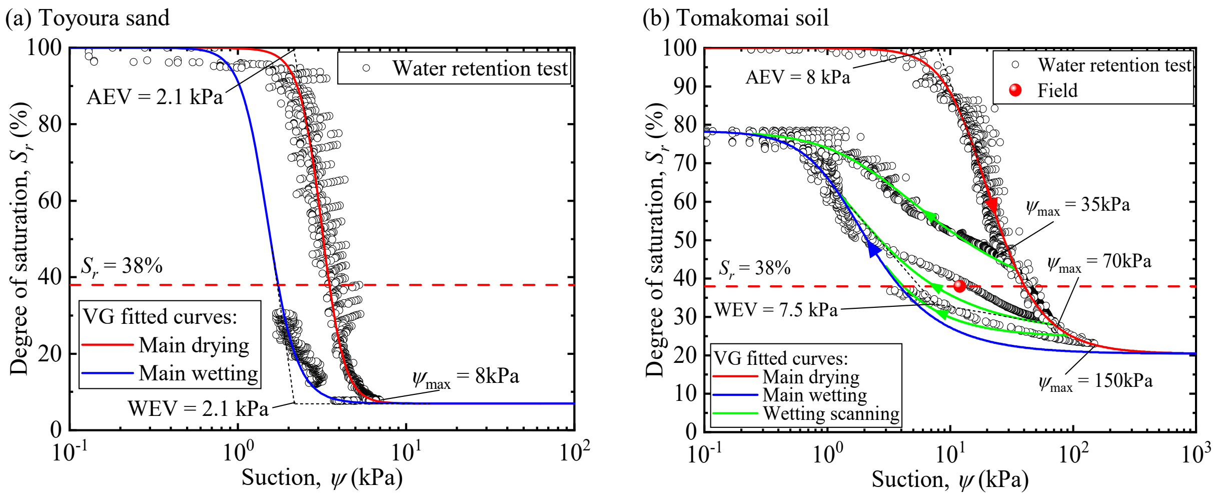

Fig. 3. SWCC of Toyoura sand and Tomakomai soil

Table 2 S_r and ψ used to investigate the effect of suction hysteresis

	ψ (kPa)	S_r (%)	SWCC Path
Toyoura sand	3.75	38	Drying
		10	Wetting
	6.10		Drying
		6	Wetting
Tomakomai soil	15	75	Drying
		38	Wetting
	50		Drying
		28	Wetting

4 Test method

4.1 Test sequence

As shown in **Fig. 4**, the freeze-thaw cyclic loading triaxial test apparatus is used to measure the resilient modulus under different climatic conditions. The air cylinder can apply cyclic axial loads through computer control. Three low-temperature baths are connected to the cap, pedestal, and cell to control the temperatures separately. The apparatus can also apply a specific matric suction by controlling the pore-air pressure from the cap and the pore-water pressure from the pedestal as shown in **Fig. 4** (b) and (c). The size of the specimen is 70mm in diameter and 170mm in height.

Fig. 5 shows the schematic diagram of the combinations of the test conditions conducted in this study. U means “unfrozen”, FT means “freeze-thaw”, and W means “wheel loading”. By combining different freeze-thaw and wheel-loading conditions, the MR tests in this study consist of five types under both saturated and unsaturated conditions: unfrozen test (hereinafter referred to as ‘U test’), unfrozen wheel loading test (hereinafter referred to as ‘UW test’), freeze-thaw test (hereinafter referred to as ‘FT test’), Freeze-thaw-wheel loading test (hereinafter referred to as ‘FTW test’), and Freeze-wheel loading-thaw test (hereinafter referred to as ‘FWT test’). U test corresponds to the normal season without wheel loading, UW test corresponds to wheel loading during the normal season, FT test corresponds to the thawing season without wheel loading, FTW test corresponds to wheel loading during the thawing season, and FWT test corresponds to wheel loading during the frozen season, respectively. Moreover, to investigate the effect of the suction hysteresis of SWCC, the unsaturated tests are divided into the drying path and the wetting path at the same suction value. The tests go through the following processes as shown in **Table 3** after the specimen is saturated by applying a back pressure of 200kPa to reach a B value of greater than 0.96.

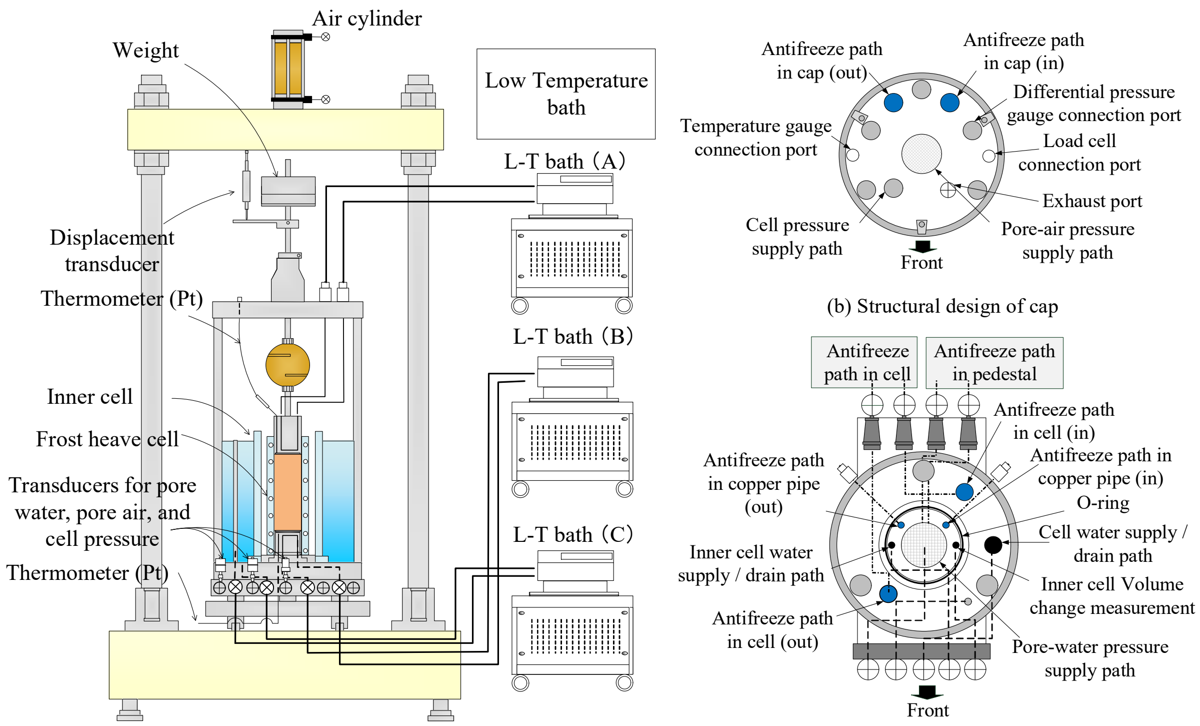

(b) Structural design of cap

(a) Schematic diagram of test apparatus (c) Structural design of pedestal

Fig. 4. Freeze-thaw cyclic loading triaxial test apparatus

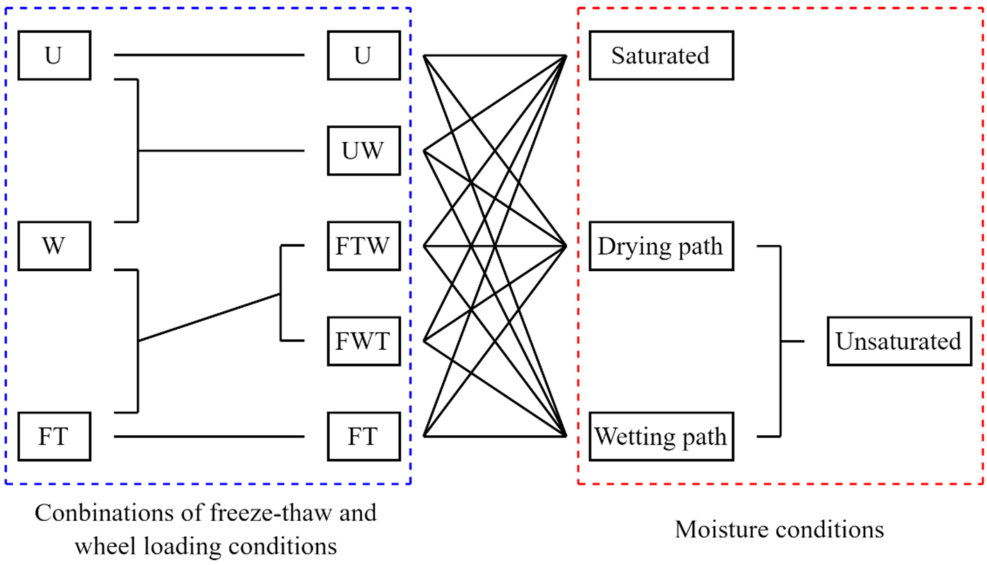

Fig. 5. Schematic diagram of combinations of test conditions

Table 3 Test sequence

Test types	Consolidation process		Unsaturation process		Freezing process		Wheel loading process		Thawing process		Wheel loading process		MR test
U	○	→	○/×	→	×	→	×	→	×	→	×	→	○
UW	○	→	○/×	→	×	→	×	→	×	→	○	→	○

FT	○	→	○/×	→	○	→	×	→	○	→	×	→ ○
FTW	○	→	○/×	→	○	→	×	→	○	→	○	→ ○
FWT	○	→	○/×	→	○	→	○	→	○	→	×	→ ○

Note: → means the direction of the test sequence; ○ means applying this progress; × means skipping this progress.

4.2 Cyclic loading conditions

The loading steps are conducted referring to the AASHTO standard T 307-99 (AASHTO, 2017). However, as shown in **Fig. 6** (a) and (b), the loading frequency in this test is 0.2 Hz due to the limitation of this test apparatus, which is different from the loading frequency of 10 Hz in the AASHTO standard. For the details, Lin et al. (2022) discussed the estimation of this limited loading frequency. However, since more study on the effect of loading frequency is necessary, the M_r results under the loading frequency of 0.2 Hz in this test are directly used without conversion. According to the AASHTO standard, there are 11 steps from MR-0 to MR-10. MR-0 is the pre-loading step to make sure the cap completely reaches the top end of the specimen. In this study, the loading number of MR-0 is determined as 2000 cycles to get a stable residual strain. Besides, since the maximum deviator stresses in MR-4, 5, 9, and 10 are larger than the field condition in Japan (Kishikawa et al., 2017), this study skips MR-4, 5, 9, and 10 and inserts MR-1.5, 2.5, 6.5, and 7.5 to keep the total number of loading step as 11. **Table 4** shows the detailed loading steps and conditions in this study.

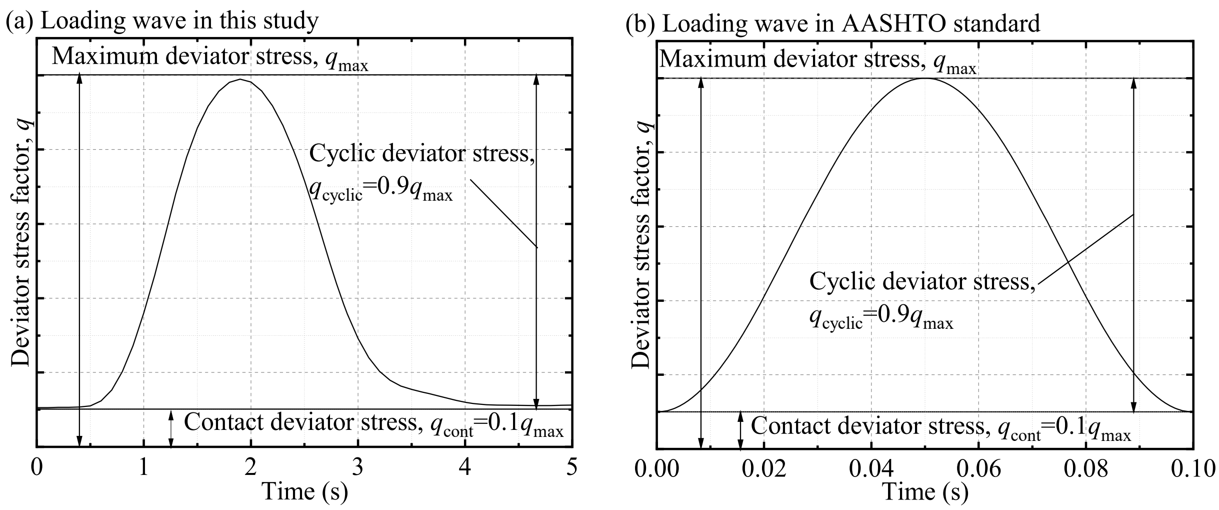

(a) Loading wave in this study (b) Loading wave in AASHTO standard

Fig. 6. Loading waves in this test and AASHTO standard

Table 4 Loading steps in MR tests

	σ_c (kPa)	q_{max} (kPa)	q_{cont} (kPa)	q_{cyclic} (kPa)	N_c
MR-0	41.4	27.6	2.76	24.84	2000
MR-1	41.4	13.8	1.38	12.42	100
MR-1.5	41.4	20.7	2.07	18.63	100
MR-2	41.4	27.6	2.76	24.84	100

MR-2.5	41.4	34.5	3.45	31.05	100
MR-3	41.4	41.4	4.14	37.26	100
MR-6	27.6	13.8	1.38	12.42	100
MR-6.5	27.6	20.7	2.07	18.63	100
MR-7	27.6	27.6	2.76	24.84	100
MR-7.5	27.6	34.5	3.45	31.05	100
MR-8	27.6	41.4	4.14	37.26	100

Note: σ_c is confining pressure; N_c is the number of loading cycles.

4.3 Moisture, wheel loading, and temperature conditions

To keep the suction constant in different stages except for freeze-thaw, the axis-translation technique is employed in this study, which was originally introduced by Hilf (1956) and widely used in unsaturated soil tests. As shown in **Fig. 7**, a membrane filter paper that is water-permeable but air-impermeable is installed at the lower end of the specimen, while a PTFE filter paper that is air-permeable but water-impermeable is installed at the upper end of the specimen. In this way, a certain suction can be determined and controlled by adjusting the pore air pressure and pore water pressure. The specifications of the filters are shown in **Table 5**. As mentioned in Section 4.1, since the initial pore air and pore water pressure are 200 kPa after the specimen is saturated, the suction can be controlled by adjusting the pore water pressure to a certain value and keeping the pore air pressure at 200 kPa. As explained in Chapter 3, to investigate the effect of the suction hysteresis of SWCC on resilient modulus, four groups of unsaturated U tests along both drying and wetting paths are conducted. Additionally, it should be noted that only the smaller suction values (Toyoura sand: 3.75 kPa; Tomakomai soil: 15 kPa) along the drying and wetting paths are adopted for other moisture conditions besides U tests.

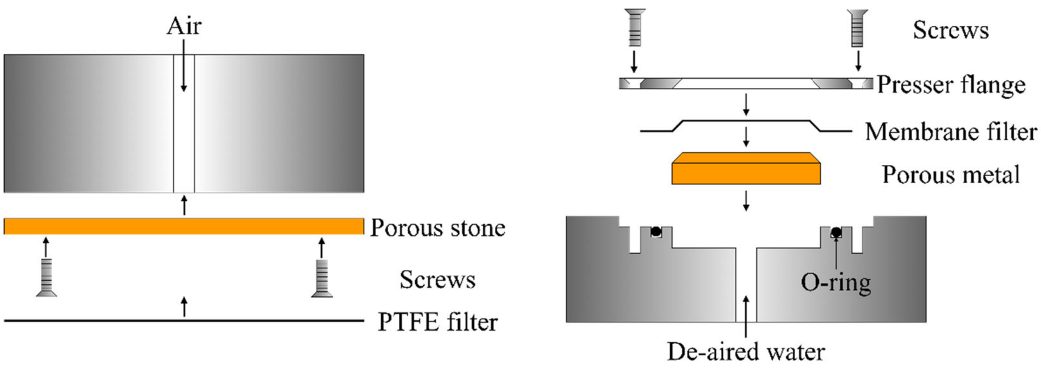

(a) Cap (b) Pedestal

Fig. 7. Installation of PTFE and membrane filters

Table 5 Specification of filters

	Material	AEV (kPa)	Thickness (μm)	Pore size (μm)

Membrane filter	Acrylic copolymer	100	94	0.45
PTFE filter	PTFE	-	135	3

The wheel loading condition in the UW, FTW, and FWT tests and the temperature condition in the FT, FTW, and FWT tests of the previous study (Lin et al., 2022) are adopted in this study. As shown in **Fig. 8**, the wheel load on the subgrade layer is caused by a 49-kN wheel load on a typical pavement structure in the Japanese design guide (Japan Road Association, 2019). When applying the standard 49-kN wheel load to the surface of the pavement, the stress transmitted to the surface of the subgrade is the cyclic deviatoric stress that should be applied in the wheel-loading process in the experiment, while the stress caused by the gravity of the pavement structure above the subgrade is the constant deviatoric stress. The cyclic deviatoric stress caused by the wheel load is calculated by the General Analysis of Multi-layered Elastic Systems (GAMES), a software to analyze the stress and strain in multi-layered pavements developed by Maina et al. (2004). As for the boundary conditions, the bottom is set as a fixed constraint boundary, while the left and right sides are set as roller constraint boundaries, respectively. Because the subgrade layer is a semi-infinite body where the distal strain of the bottom should converge to zero, while the left and the right sides of the whole pavement structure are also infinite where the horizontal distal strain should converge to zero but free in the vertical direction. q_{cont} and q_{cyclic} are determined as 9.6 and 26.2 kPa in the thawing season, and 9.6 and 24.5 kPa in the frozen season. The loading frequency and waveform are the same as in the MR test, and the loading number is 1000.

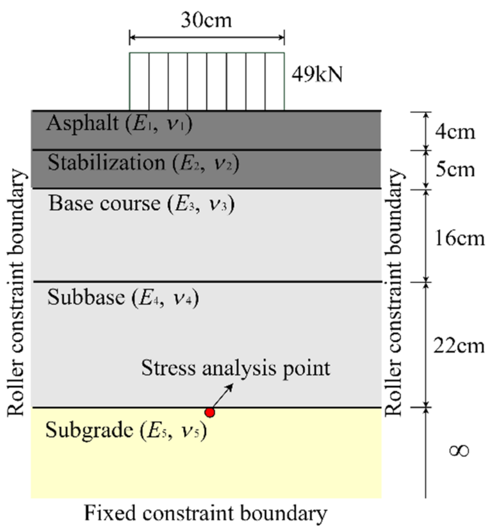

Fig. 8. Pavement structure and wheel loading conditions

According to the Japanese standard JGS 0172 (Japanese Geotechnical Society, 2018), a one-dimensional freeze-thaw action is conducted in an open system with axial stress of 10 kPa for the FT, FTW, and FWT tests. The temperature change in the freeze-thaw process is shown in **Fig. 9**.

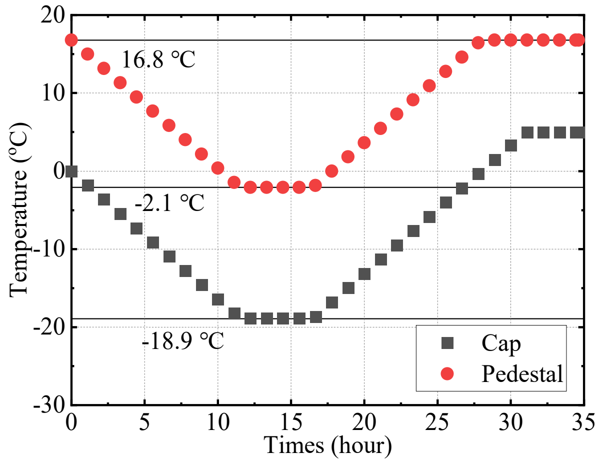

Fig. 9. Temperature change in the freeze-thaw process

4.4 Effect of freeze-thaw and wheel load on moisture change

Fig. 10 and **Fig. 11** show the water drainage and frost heave during the freeze-thaw process and the water drainage during the wheel-loading process, respectively. From **Fig. 10**, it can be found that although the water content changes during the freeze-thaw process, especially in the saturated specimens, the final change returns to about zero. In the unsaturated tests along drying and wetting paths, the change in the water during the freeze-thaw process is insignificant because the water content of the specimen is small. Similarly, it can be found from **Fig. 11** that the change in the water content caused by the wheel loading process is also small. **Table 6** shows the change ratios of water contents by freeze-thaw and wheel load compared to the initial water contents. In general, the change in the water content caused by the freeze-thaw and wheel-loading processes is less than 2% compared to the initial water content, which is negligible.

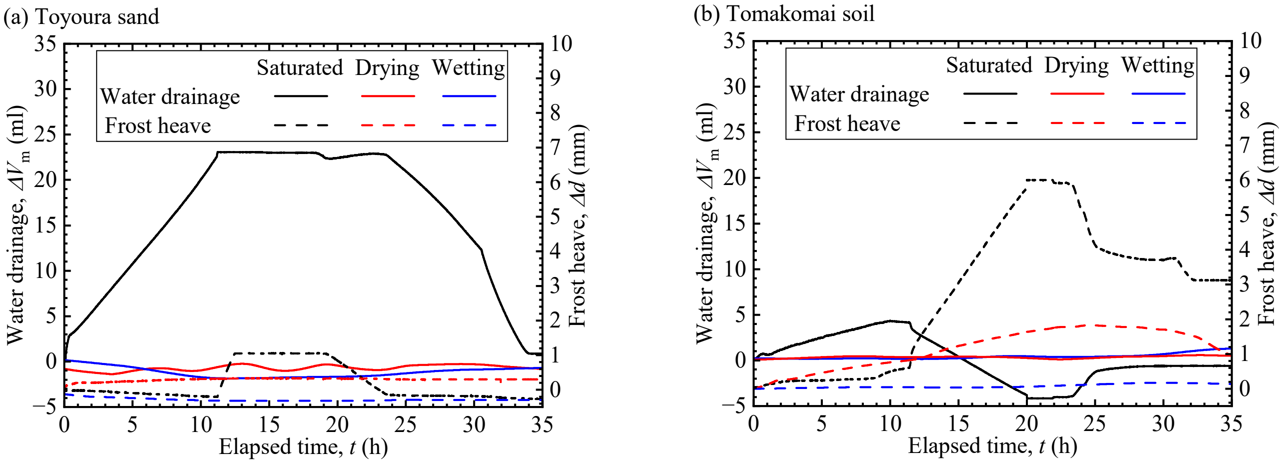

Fig. 10. Water drainage and frost heave during the freeze-thaw process (FT test)

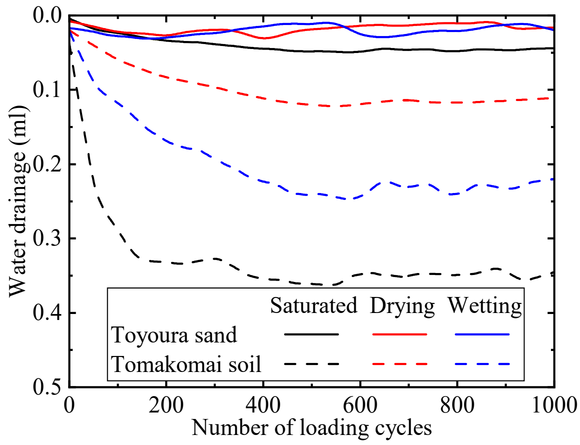

Fig. 11. Water drainage during the wheel loading process (UW test)

Table 6 Water content change by freeze-thaw and wheel load

	Moisture condition	Suction (kPa)	Initial water content	Change ratio caused by freeze-thaw (%)	Change ratio caused by wheel load (%)
Toyoura sand	Saturated	0	0.268	0.31	0.015
	Drying path	3.75	0.107	0.78	0.015
	Wetting path	3.75	0.027	1.75	0.073
Tomakomai soil	Saturated	0	0.448	0.17	0.098
	Drying path	15	0.336	0.20	0.083
	Wetting path	15	0.152	1.07	0.091

5 Test results and discussions

5.1 U test

Fig. 12 shows the measured resilient moduli of the saturated and unsaturated U tests under different degrees of saturation and matric suctions. The X-axis is the peak deviator stress applied to the specimen during the loading process, the Y-axis is the confining pressure, and the Z-axis is the measured resilient modulus. Generally, resilient modulus increases with the increment of the confining pressure and the matric suction but decreases with the increment of the deviator stress.

To compare the test results and analyze the effects under different matric suction values, all the test results are fitted by regression analysis through Lin's climatic Ng model shown in **Eq. 4**. It should be noted that all the test results under different suction values are fitted together so that one set of parameters can represent various moisture conditions. The test results with fitting surfaces and parameters of regression analysis are shown in **Fig. 12** and **Table 7**, respectively. It can be found that although the degrees of saturation under the same matric suction differ along the drying and wetting paths, the measured resilient moduli are very close. The effect of suction hysteresis on the M_r at the same suction value along different drying and wetting paths is complicated and may differ in different materials and mechanical conditions, which can be illustrated as a three-dimensional relationship with respect to moisture content and suction (Khoury & Zaman, 2004). Khoury et al. (2011) found that the M_r along the wetting path is higher than that along the drying path at the same suction based on tests with manufactured soil, which can be explained by the possible water content lubricant effect. Ng et al. (2013) observed a similar phenomenon with low cyclic stress based on tests with a completely decomposed tuff sampled from Hong Kong but found the effect becomes less significant with an increase in cyclic stress. A similar phenomenon can also be observed in this study, especially as shown in **Fig. 12 (b)**. However, since the difference of M_r between the drying and wetting paths is insignificant under the tested level in this study, the M_r along the drying and wetting paths can be fitted together with respect to the same matric suction. This is also consistent with the fact that the Ng model only considers the matric suction ψ but not the moisture content as the parameter to predict the resilient modulus of partly saturated soils (Ng et al., 2013).

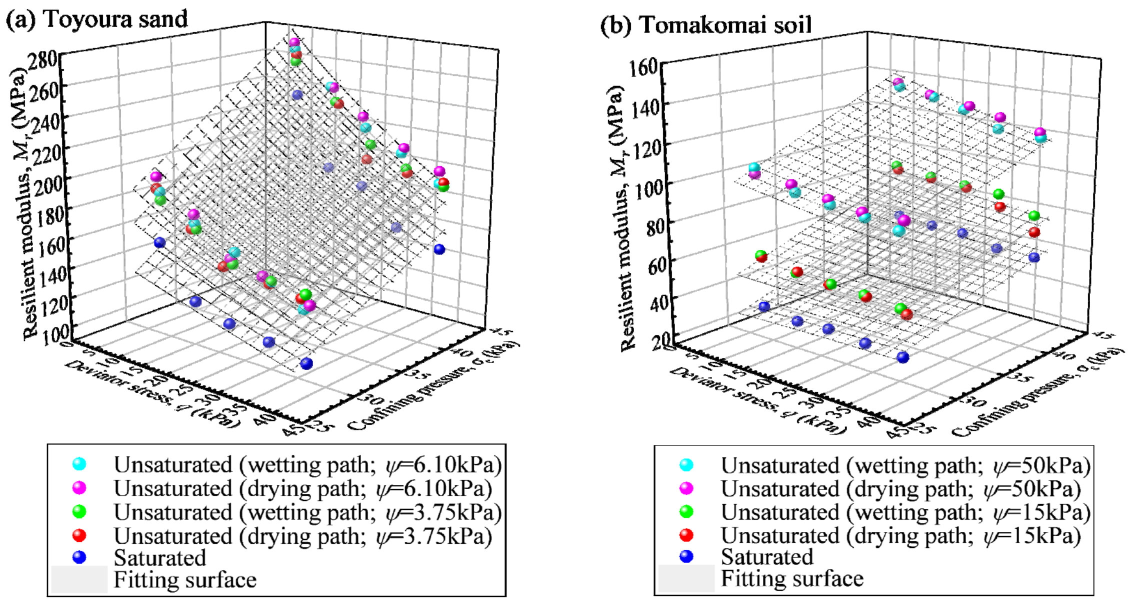

Fig. 12. Results of U tests for Toyoura sand and Tomakomai soil

Table 7 Regression analysis results of U tests

	F_{clim}	k_1	k_2	k_3	k_4	R^2
Toyoura sand	1	2.089	1.057	-4.437	1.692	0.948
Tomakomai soil	1	0.526	1.293	-2.650	1.008	0.988

5.2 UW test

Similar to the results of the U test, the results of the UW test with Lin's climatic Ng model fitted surfaces and parameters of regression analysis are shown in **Fig. 13** and **Table 8**, respectively. To compare the resilient moduli of the U test and UW test, the resilient moduli of the UW/U test for both Toyoura sand and Tomakomai soil are shown in **Fig. 14**. It can be found that all the scatters of Toyoura sand are below the 1:1 line but those of Tomakomai soil are upon the 1:1 line, which indicates that the wheel loading process increases the resilient modulus of Tomakomai soil but decreases that of Toyoura sand.

To discuss the effect of traffic load on the different results in Toyoura sand and Tomakomai soil, the water drainage that reflects the volumetric change of the soil sample during the wheel loading process is recorded. **Fig. 11** plots the water drainage after every loading cycle during the wheel loading process for Toyoura sand and Tomakomai soil. As shown in **Fig. 11**, the water drainage during the wheel loading process is nearly a typical consolidation curve. This is because the relatively high q_{cont} of 9.6 kPa will lead to a consolidation of the soil specimen during the wheel loading process. In the case of Tomakomai soil, the increment of the sample density indirectly increases the soil strength, which leads to an increment of the M_r. However, the water drainage of Toyoura sand during the wheel loading process is much less compared with Tomakomai soil, which indicates that the consolidation effect of Toyoura sand during the wheel loading process is less than Tomakomai soil. Furthermore, since Toyoura sand is much more poorly graded than Tomakomai soil as shown in **Fig. 1**, the soil skeleton may be disturbed by the wheel loading process due to the lack of fine fraction, which leads to a decrement of the resilient modulus. This kind of decrement in resilient modulus caused by wheel loads is also explained as the disturbance of soil particle skeleton structure uniformity by Lin et al. (2022).

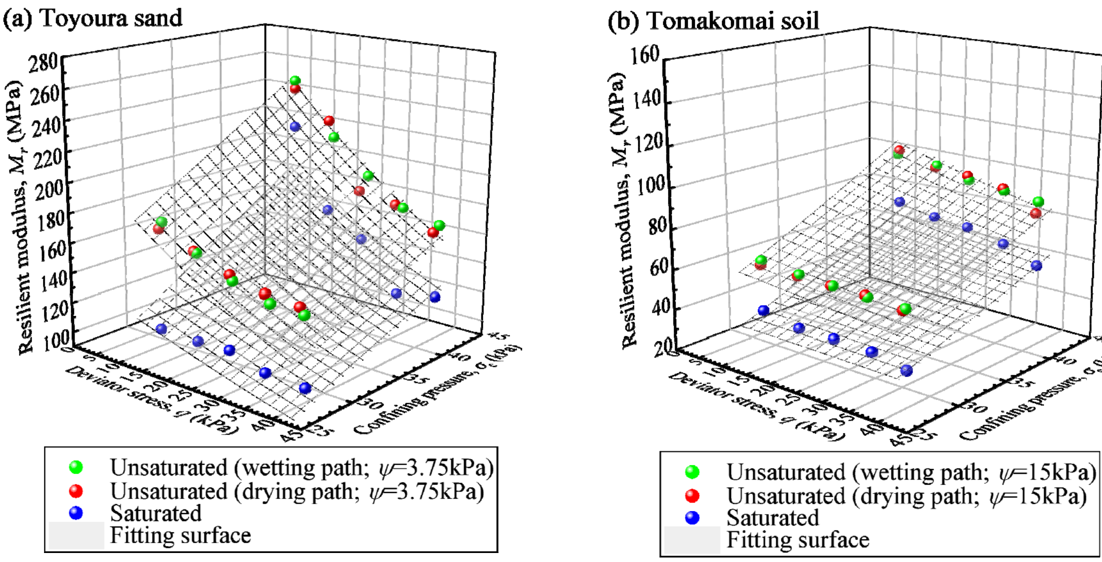

Fig. 13. Results of UW tests for Toyoura sand and Tomakomai soil

Table 8 Regression analysis results of UW tests

	F_{clim}	k_1	k_2	k_3	k_4	R^2
Toyoura sand	1	1.750	1.088	-4.916	3.639	0.905
Tomakomai soil	1	0.568	1.541	-3.658	1.258	0.985

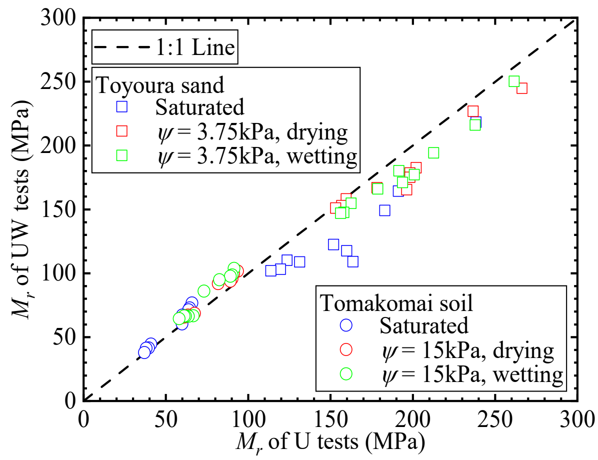

Fig. 14. Resilient moduli of UW/U tests

5.3 FT test

As shown in **Fig. 15**, the results along the drying and wetting paths are significantly different in the case of FT tests. This is because different moisture contents, although the matric suction is the same, will cause different freeze-thaw effects, as shown in **Fig. 11**, where it can be found that the frost heave decreases with the decrement of the water content. In addition, the frost susceptibility of Tomakomai soil is significantly greater than that of Toyoura sand. Therefore, the FT test results under different water contents and frost heave amounts are separately fitted by regression analysis using Lin's climatic Ng model. It is noted that to keep the consistency of the tests with and without the freeze-thaw process, the FT test utilized the same regression parameters of k_1 to k_4 as the U test. **Table 9** shows the regression analysis results of FT tests for Toyoura sand and Tomakomai soil. As shown in **Fig. 16**, it can be found that the freeze-thaw process generally decreases the resilient modulus, which is obvious because the formation of ice disturbs the original soil skeleton. Furthermore, the parameter F_{clim} decreases with the decrement of moisture content and is affected by the moisture content, which also indicates that the effect of freeze-thaw action on resilient modulus is positively correlated with moisture content. As shown in **Fig. 10**, the axial strain would increase, and the specimen would drain or absorb a certain amount of water during the freezing process. Meanwhile, the axial strain and the amount of absorbed water were also affected by the water content of the specimen. After thawing, the axial strain would decrease but not restore to the original height, which lead to a rearrangement of the soil skeleton. Furthermore, many researchers have observed changes in soil structure caused by freeze-thaw actions at the microscopic level using methods such as X-ray (Starkloff et al., 2017; Wang et al., 2018; Leuther and Schlüter, 2021). Although the frost heave differs a lot, the average decreasing rates of M_r of Toyoura sand and Tomakomai soil are 6.8% and 5.6%, respectively. The possible reason why the M_r of Toyoura sand has a greater decreasing rate than Tomakomai soil is that as a poorly graded sand, the soil skeleton of Toyoura sand is more susceptible to disturbance. From the comparison of the M_r decreasing rates of Toyoura sand and Tomakomai soil, it can be found that the effect of freeze-thaw action on the M_r of frost-susceptible soil is not greater than non-frost-susceptible one, which indicates that the greatest harm of the freeze-thaw action to the pavement with frost-susceptible subgrade soil is the structural damage to the pavement structure due to the significant frost heave.

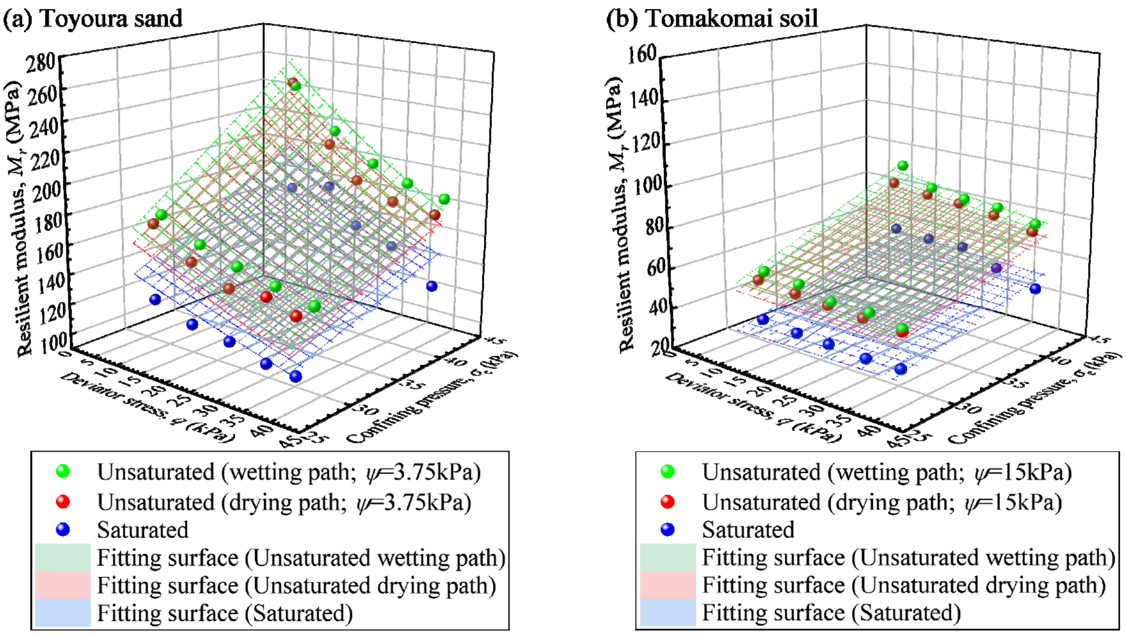

Fig. 15. Results of FT tests for Toyoura sand and Tomakomai soil

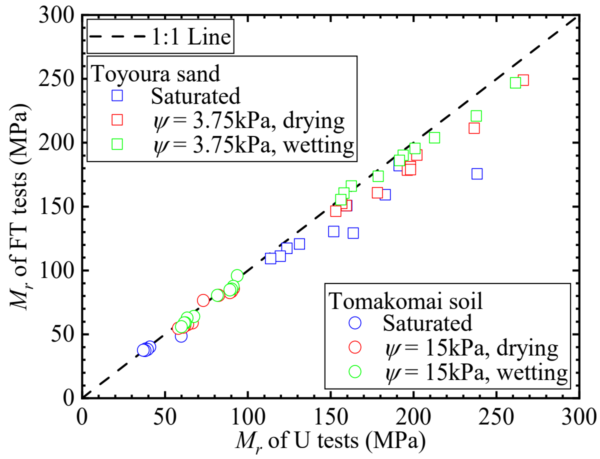

Fig. 16. Resilient moduli of FT/U tests

Table 9 Regression analysis results of FT tests

Material	Moisture condition		F_{clim}	k_1	k_2	k_3	k_4	R^2
Toyoura sand	Saturated		0.810	2.089	1.057	-4.437	1.692	0.941
	Unsaturated	Drying path	0.939	2.089	1.057	-4.437	1.692	0.928
		Wetting path	0.997	2.089	1.057	-4.437	1.692	0.876
Tomakomai soil	Saturated		0.908	0.526	1.293	-2.650	1.008	0.961
	Unsaturated	Drying path	0.962	0.526	1.293	-2.650	1.008	0.984
		Wetting path	0.992	0.526	1.293	-2.650	1.008	0.968

5.4 FTW test

The results of FTW tests for Toyoura sand and Tomakomai soil are shown in **Fig. 17**. **Fig. 18** shows that there are certain relationships between the U/UW test and the FTW test. However, in the comparison between the FTW and U tests in **Fig. 18 (a)**, the scatters of Toyoura sand and Tomakomai soil are located at different sides of the 1:1 line, making it difficult to determine whether the ‘freeze-thaw-wheel loading’ process increases or decreases the resilient modulus. On the other hand, in the comparison between the FTW and UW tests in **Fig. 18 (b)**, the 1:1 line is located at the center of the scatters of both Toyoura sand and Tomakomai soil, indicating that the results of FTW tests are close to the UW tests. The possible reason for this is similar to the UW test: the consolidation plays a leading role in increasing the resilient modulus after freeze-thaw in the case of Tomakomai soil, but the disturbance of the soil skeleton plays a leading role in decreasing the resilient modulus in the case of Toyoura sand. Therefore, using the same predicting parameters as the UW test for FTW test is considered to be reasonable.

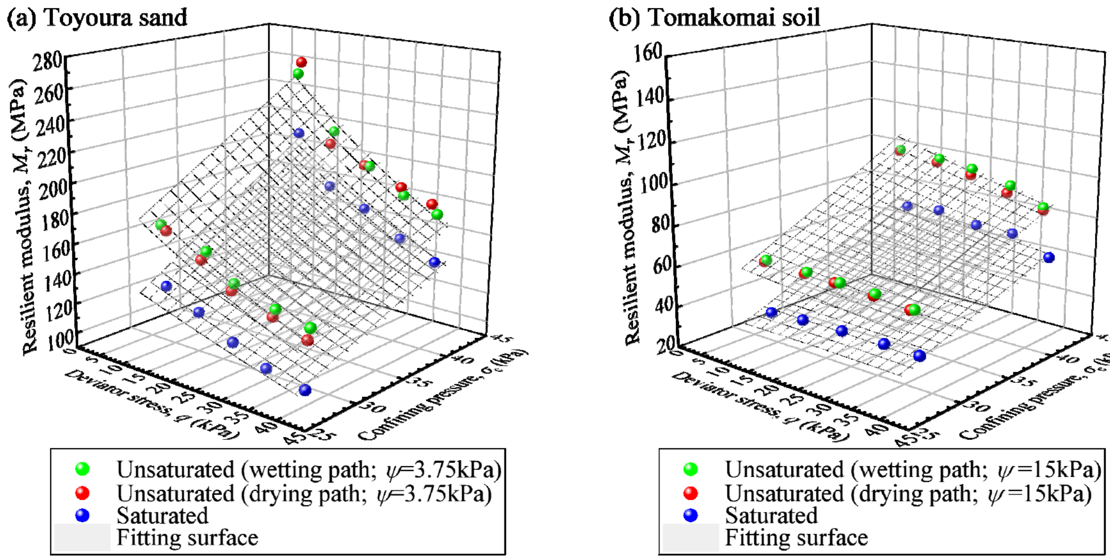

Fig. 17. Results of FTW tests for Toyoura sand and Tomakomai soil

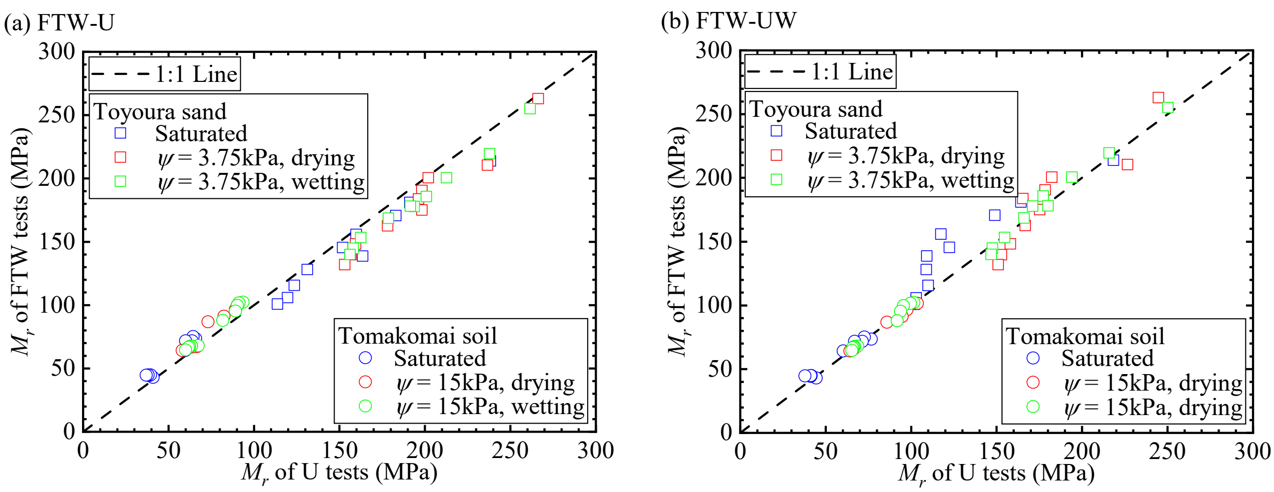

Fig. 18. Resilient moduli of FTW/U and FTW/UW tests

5.5 FWT test

Fig. 19 shows the results of FWT tests for Toyoura sand and Tomakomai soil. Compared with the results of FT tests shown in **Fig. 15**, it can be found that the results of FWT tests and FT tests are nearly identical. As shown in **Fig. 20**, the 1:1 line is located at the center of the scatters of both Toyoura sand and Tomakomai soil, also indicating that the resilient moduli of FWT and FT tests are similar. From these results, it can be inferred that the effect of the wheel loading process during the frozen season may be minimal because of the extremely high stiffness of the soil compared to normal seasons due to the freezing of water. Lin et al. (2022) have also compared the secant Young's moduli and axial strains of the frozen season and the thawing season during the wheel loading processes and found that the secant Young's modulus of the frozen season is far greater than that of the thawing season, whereas the permanent axial strain and the maximum axial strain of the frozen season are both far less than those of the thawing season. Therefore, using the same predicting parameters as the FT test for FWT test is considered to be reasonable.

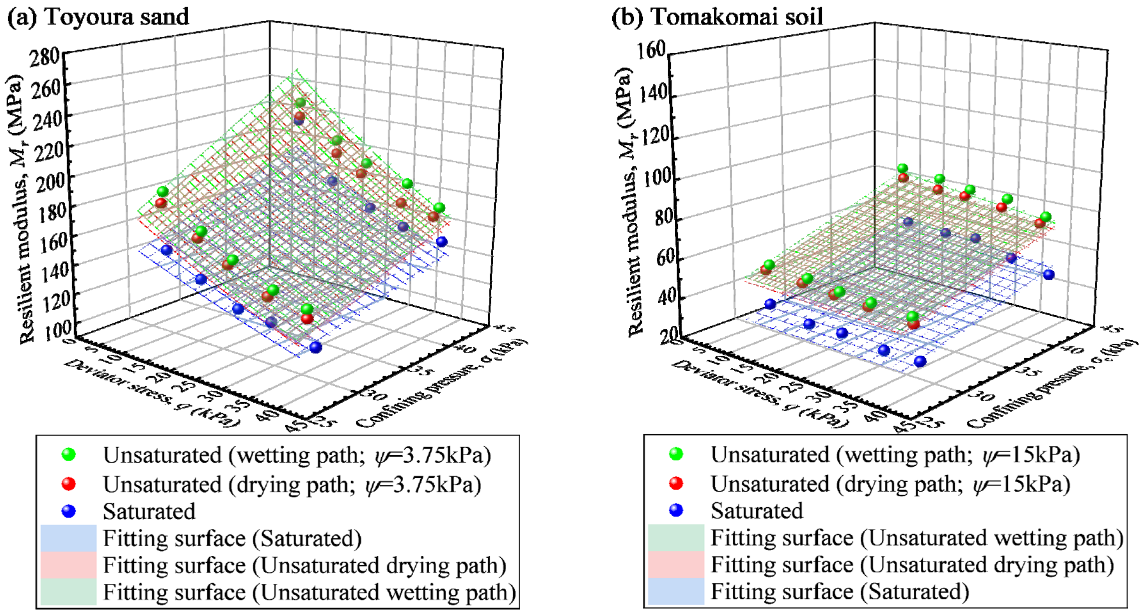

Fig. 19. Results of FWT tests for Toyoura sand and Tomakomai soil

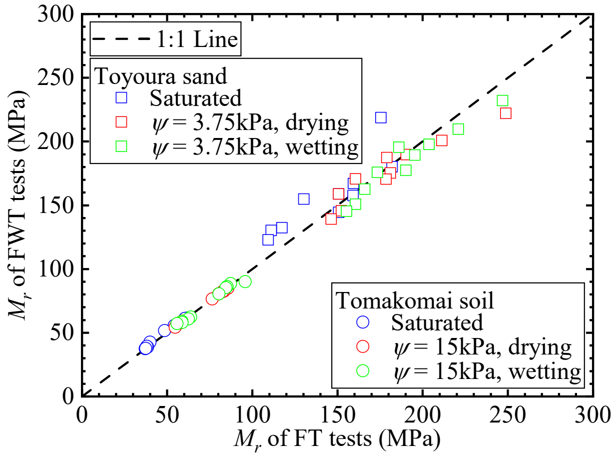

Fig. 20. Resilient moduli of FWT/FT tests

6 Conclusions

In this study, M_r tests under different moisture, wheel loading, and temperature conditions are conducted to investigate the effect of complex environmental conditions on the resilient modulus of both non-frost-susceptible and frost-susceptible subgrade soils. Based on the test results and discussions from this study, the following findings can be mainly drawn:

- Generally, M_r increases with the increment of the confining pressure and the matric suction but decreases with the increment of the deviator stress. In saturated and unsaturated soils, the matric suction plays a leading role in the change of M_r under different moisture conditions. The effect of suction hysteresis on the M_r at the same suction value along different drying and wetting paths is complicated and may differ in different materials, mechanical conditions, and temperature conditions.
- During the normal season, the effect of wheel load may differ in different materials. In the case of Tomakomai soil, the increment of the sample density indirectly increases the soil strength, which leads to an increment of the resilient moduli. However, the water drainage of Toyoura sand during the wheel loading process is much less compared with Tomakomai soil, which indicates that the consolidation effect of Toyoura sand during the wheel loading process is less than Tomakomai soil. Furthermore, since Toyoura sand is much more poorly graded, the soil skeleton may be disturbed by the wheel loading process due to the lack of fine fraction, which leads to a decrement of the resilient modulus.

- During the thawing season, since although the matric suction is the same, different moisture contents will cause different freeze-thaw effects, the M_r along the drying and wetting paths are significantly different. The freeze-thaw process generally decreases the M_r, which is obvious because the formation of ice disturbs the original soil skeleton. Furthermore, the effect of freeze-thaw action on resilient modulus is positively correlated with moisture content.
- Although the frost heave differs a lot, the average decreasing rates of M_r of Toyoura sand and Tomakomai soil are 6.8% and 5.6%, respectively. It can be found that the effect of freeze-thaw action on the M_r of frost-susceptible soil is not greater than non-frost-susceptible one, which indicates that the greatest harm of the freeze-thaw action to the pavement with frost-susceptible subgrade soil is the structural damage to the pavement structure due to the significant frost heave.
- The effect of combinations of freeze-thaw action and wheel load is more complicated, which comprehensively depends on the wheel loading sequence and material properties. On the one hand, the results of FTW tests are close to the UW tests. The possible reason is similar to the UW test: the consolidation plays a leading role in increasing the resilient modulus after freeze-thaw in the case of Tomakomai soil, but the disturbance of the soil skeleton plays a leading role in decreasing the resilient modulus in the case of Toyoura sand. On the other hand, the results of FWT and FT tests are similar. It can be inferred that the effect of the wheel loading process during the frozen season may be minimal because of the extremely high stiffness of the soil compared to normal seasons due to the freezing of water. Therefore, using the same predicting parameters as the UW tests for FTW tests and the same predicting parameters as the FT tests for FWT tests is considered to be reasonable.

Acknowledgment

This research was supported in part by Grant-in-Aid for Scientific Research (B) (19H02234) and (A) (20H00266) from Japan Society for the Promotion of Science (JSPS) KA-KENHI. The provision of the continuous pressurization water retention test apparatus by Prof. Satoshi Nishimura is highly acknowledged by the authors. Support from JST SPRING Grant Number JPMJSP2119 is also highly acknowledged.

References

AASHTO. AASHTO Guide for Design of Pavement Structures. Washington, D.C.: AASHTO; 1986.

AASHTO. Standard method of test for determining the resilient modulus of soils and aggregate materials. Washington, D.C.: AASHTO; 2017. https://doi.org/10.1520/STP12519S

AASHTO. Mechanistic-empirical pavement design guide: a manual of practice. Washington, D.C.: AASHTO; 2020.

Alowaisy, A., Yasufuku, N., Ishikura, R., Hatakeyama, M., and Kyono, S. Continuous pressurization method for a rapid determination of the soil water characteristics curve for remolded and undisturbed cohesionless soils. Soils and Foundations. 2020; 60(3): 634-647. https://doi.org/10.1016/j.sandf.2020.03.014.

ASTM. Standard practice for classification of soils for engineering purposes (unified soil classification system), ASTM Int'l; 2017. https://doi.org/10.1520/D2487-17.

Berg, R.L., Bigl, S.R., Stark, J.A., and Durell, G.D. Resilient Modulus Testing of Materials from Mn/Road, Phase 1. 1996. https://doi.org/10.21949/1404573.

Brown, S. Soil mechanics in pavement engineering. Geotechnique. 1996; 46(3): 383-425. https://doi.org/10.1680/geot.1996.46.3.383.

Cole, D.M., Irwin, L.H., and Johnson, T.C. Effect of freezing and thawing on resilient modulus of a granular soil exhibiting nonlinear behavior. Transportation Research Record. 1981.

Fredlund, D.G., Rahardjo, H., and Fredlund, M.D. Unsaturated soil mechanics in engineering practice. John Wiley & Sons, Hoboken, N.J.; 2012.

Gu, F., Sahin, H., Luo, X., Luo, R., and Lytton, R.L. Estimation of Resilient Modulus of Unbound Aggregates Using Performance-Related Base Course Properties. Journal of Materials in Civil Engineering. 2015; 27 (6): 04014188. https://doi.org/10.1061/(asce)mt.1943-5533.0001147.

Gupta, S., Ranaivoson, A., Edil, T., Benson, C., and Sawangsuriya, A. Pavement design using unsaturated soil technology. St. Paul, Minnesota: Minnesota Department of Transportation; 2007.

Han, Z., and Vanapalli, S. State-of-the-Art: Prediction of Resilient Modulus of Unsaturated Subgrade Soils. International Journal of Geomechanics. 2016; 16(4). https://doi.org/10.1061/(ASCE)GM.1943-5622.0000631.

Hatakeyama, M., Kyono, S., and Kawahara, T. Development of Water Retention Test Apparatus According to The Continuous Pressurization Method. Oyo technical report. 2015; (34): 23-54.

Heath, A., Pestana, J., Harvey, J., and Bejerano, M. Normalizing behaviour of unsaturated granular pavement materials. Journal of Geotechnical and Geoenvironmental Engineering. 2004; 130(9): 896-904. https://doi.org/10.1061/(ASCE)1090-0241(2004)130:9(896).

Hilf, J.W. 1956. An investigation of pore-water pressure in compacted cohesive soils. Ph.D., University of Colorado at Boulder. Colorado, United States.

Ishikawa, T., Lin, T., Kawabata, S., Kameyama, S., and Tokoro, T. Effect evaluation of freeze-thaw on resilient modulus of unsaturated granular base course material in pavement. Transportation Geotechnics. 2019; 21. https://doi.org/10.1016/j.trgeo.2019.100284.

Japanese Geotechnical Society. Laboratory testing standards for geomaterials. Japanese Geotechnical Society Standards. Tokyo: Maruzen; 2018.

Japan Road Association. Handbook for asphalt pavement. Tokyo: Maruzen; 2019.

Johnson, T.C., Cole, D.M., Chamberlain, E.J. Influence of Freezing and Thawing on the Resilient Properties of a Silt Soil Beneath an Asphalt Concrete Pavement. CRREL report, The Laboratory. 1978.

Kato, S., Hatakeyama, M., Abe, H., Kim, B., and Takeshita, Y. Measurement of Soil-Water Characteristic Curve with a continuous pressurization method. *In* Unsaturated Soil Mechanics-from Theory to Practice: Proceedings of the 6th Asia Pacific Conference on Unsaturated Soils (Guilin, China, 23-26 October 2015). 2015. CRC Press. p. 379.

Khoury, C., Khoury, N., and Miller, G. Effect of Cyclic Suction History (Hydraulic Hysteresis) on Resilient Modulus of Unsaturated Fine-Grained Soil. Transportation Research Record. 2011; 2232(1): p. 68-75. https://doi.org/10.3141/2232-07.

Khoury, N., Brooks, R., and Khoury, C. Environmental influences on the engineering behavior of unsaturated undisturbed subgrade soils: effect of soil suctions on resilient modulus. International Journal of Geotechnical Engineering. 2009; 3(2): 303-311. https://doi.org/10.3328/IJGE.2009.03.02.303-311.

Khoury, N., and Zaman, M., Correlation Between Resilient Modulus, Moisture Variation, and Soil Suction for Subgrade Soils. Transportation Research Record. 2004; 1874(1): 99-107. https://doi.org/10.3141/1874-11.

Kim, B., Hatakeyama, M., Park, S., Park, H., Takeshita, Y., and Kato, S. Assessment of Water Retention Test by Continuous Pressurization Method . Geotechnical Testing Journal. 2021; 44(2): 274-289. https://doi.org/10.1520/GTJ20190410.

Kim, D., and Kim, J. Resilient behavior of compacted subgrade soils under the repeated triaxial test. Construction and Building Materials. 2007; 21(7): 1470-1479. https://doi.org/10.1016/j.conbuildmat.2006.07.006.

Kishikawa, T., Otgonjargal, D., Kawaguchi, T., Nakamura, D., and Yamashita, S. Influence of freeze-thaw on stress propagation in the ground. 57th Technical Report of the Annual Meeting of the JGS Hokkaido Branch. 2017; 27-34. (In Japanese).

Leuther, F., and Schlüter, S. Impact of freeze–thaw cycles on soil structure and soil hydraulic properties. SOIL. 2021; 7(1): 179-191. https://doi.org/10.5194/soil-7-179-2021.

LI, D., and SELIG, E. Resilient modulus for fine-grained subgrade soils. Journal of Geotechnical Engineering-Asce. 1994; 120(6): 939-957. https://doi.org/10.1061/(ASCE)0733-9410(1994)120:6(939).

Liang, R., Rabab'ah, S., and Khasawneh, M. Predicting moisture-dependent resilient modulus of cohesive soils using soil suction concept. Journal of Transportation Engineering. 2008; 134(1): 34-40. https://doi.org/10.1061/(ASCE)0733-947X(2008)134:1(34).

Lin, T.S., Ishikawa, T., Maruyama, K., and Tokoro, T. Pavement design method in Japan with consideration of climate effect and principal stress axis rotation. Transportation Geotechnics. 2021; 28. https://doi.org/10.1016/j.trgeo.2021.100552.

Lin, T., Ishikawa, T., Yang, J., and Tokoro, T. Evaluation of climate effect on resilient modulus of granular subgrade material. Cold Regions Science and Technology. 2022; 194. https://doi.org/10.1016/j.coldregions.2021.103452.

Lu, N., and Likos, W.J. Unsaturated soil mechanics. J. Wiley, Hoboken, N.J.; 2004.

Lytton, R. L. Foundations and pavements on unsaturated soils. Proceedings of the 1st International Conference on Unsaturated Soils. UNSAT 95. 1996; 3: 1201-1220.

Maina, J., and Matsui, K. Developing software for elastic analysis of pavement structure responses to vertical and horizontal surface loadings. Transportation Research Record. 2004; 1896(1): 107-118. https://doi.org/10.3141/1896-11

NCHRP, and ARA, Inc. Final report. Guide for mechanistic-empirical pavement design of new and rehabilitated pavement structures. 2004.

Ng, C., Zhou, C., Yuan, Q., and Xu, J. Resilient modulus of unsaturated subgrade soil: experimental and theoretical investigations. Canadian Geotechnical Journal. 2013; 50(2): 223-232. https://doi.org/10.1139/cgj-2012-0052.

Oh, J., Fernando, E., Holzschuher, C., and Horhota, D. Comparison of resilient modulus values for Florida flexible mechanistic-empirical pavement design. International Journal of Pavement Engineering. 2012; 13(5): 472-484. https://doi.org/10.1080/10298436.2011.633170.

Sahin, H., Gu, F., Tong, Y., Luo, R., and Lytton, R. Unsaturated soil mechanics in the design and performance of pavements. Advances in Unsaturated Soils - Proceedings of the 1st Pan-American Conference on Unsaturated Soils, PanAmUNSAT 2013. 2013; 87-99. https://doi.org/10.1201/b14393-8.

Seed, H.B., Chan, C.K., and Monismith, C.L. Effects of repeated loading on the strength and deformation of compacted clay. Thirty-Fourth Annual Meeting of the Highway Research Board. 1955; 541-558.

Simonsen, E., and Isacsson, U. Soil behavior during freezing and thawing using variable and constant confining pressure triaxial tests. Canadian Geotechnical Journal. 2001; 38(4): 863-875. https://doi.org/10.1139/t01-007.

Simonsen, E., Janoo, V., and Isacsson, U. Resilient properties of unbound road materials during seasonal frost conditions. Journal of Cold Regions Engineering. 2002; 16(1): 28-50. https://doi.org/10.1061/(ASCE)0887-381X(2002)16:1(28).

Starkloff, T., Larsbo, M., Stolte, J., Hessel, R., and Ritsema, C. Quantifying the impact of a succession of freezing-thawing cycles on the pore network of a silty clay loam and a loamy sand topsoil using X-ray tomography. Catena. 2017; 156: 365-374. https://doi.org/10.1016/j.catena.2017.04.026.

VanGenuchten, M. A Closed-form equation for predicting the hydraulic conductivity of unsaturated soils. Soil Science Society of America Journal. 1980; 44(5): 892-898. https://doi.org/10.2136/sssaj1980.03615995004400050002x.

Wang, S., Yang, P., and Yang, Z. Characterization of freeze-thaw effects within clay by 3D X-ray Computed Tomography. Cold Regions Science and Technology. 2018; 148: 13-21. https://doi.org/10.1016/j.coldregions.2018.01.001.

Yasuoka, T., Ishikawa, T., Wu, Y., Tokoro, T., Maruyama, K., and Ueno, C. Proposal of installation method of geosynthetics drainage material for frost heave depression of road pavement. *In* Japanese Geotechnical Society Hokkaido Branch Technical Report Collection. Hokkaido, Japan. 2021; 61: 155-164.